A Feasibility Study of Customized and Fully Aerosol-Jet-Printed Micro-Electrode Arrays for In Vitro Application

Ileana Armando, *Student Member, IEEE*, Michela Borghetti, *Member, IEEE*, Emilio Sardini, *Senior Member, IEEE*, and Mauro Serpelloni, *Member, IEEE*

***Abstract*—The article proposes a fully printed microelectrode array (MEA) as a proof of concept for the feasibility of a customized and low-cost bioelectronic device. The target application is to promote the maturation of the cell culture by providing biophysical stimuli and evaluating the functionality of the bioengineered products, monitoring in real-time the electrogenic cell action potential. The MEA is entirely printed with aerosol jet printing (AJP) with a multilayer structure composed of an array of 16 electrodes. AJP fabrication was exploited as low-cost technique and easy and reliable possibility to print both insulated material and conductive polymer. Furthermore, the technique allows the realization of a customized electrode design according to specific neuronal network architecture. The chosen inks achieve the requirements for the intended use, in terms of high conductivity for electrodes, low conductivity for passivation layers, and biocompatibility for cell culture. Results from geometrical characterization showed an agreement with the design requirements. In particular, the first prototypes showed a thickness of the passivation layer of (33.4 ± 1.4) μm and the silver conductive tracks with a thickness of (5.5 ± 0.6) μm and a width of (68 ± 1.4) μm. Electrochemical Impedance Spectroscopy established an impedance magnitude value significantly below compared with commercial MEA and inkjet printing MEA. The reusability and the stability of the sensor are demonstrated within two weeks. Overall, the results suggest the possibility to exploit the potential to print MEA onto platform, for in vitro cell culture and to integrate other types of biosensors.**

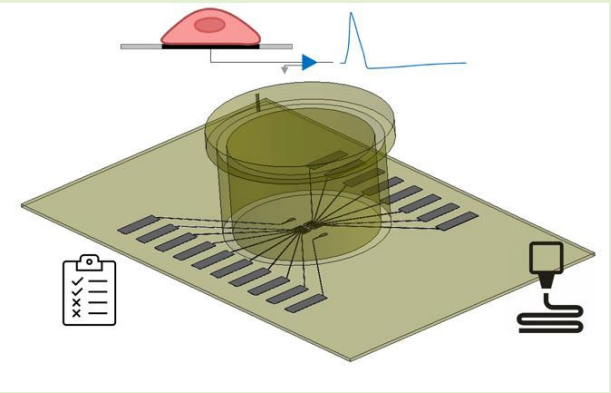

***Index Terms*— Additive manufacturing (AM), aerosol jet printing (AJP), biomedical application, biosensor, in vitro cell culture, microelectrode array (MEA), printed sensor.**

I. Introduction

IN VITRO electrophysiological recordings are an important step in the study of physiological and pathological models of neuronal cells and electrogenic cells in general, which generate these signals [1]. As well as being a significant tool for the realization of functional tissue and engineering products [2]. The electrophysiological signal generated by an asymmetry of charges on each side of the semipermeable cell membrane creates a difference in electrical potential. The electrochemical gradient generates currents, due to ionic movements throw the cell membrane. Traditional intracellular recording techniques such as patch clamp, an intracellular measurement on a single cell at once with an invasive method, provide a better signal quality but limit the recording number of neuronal signals [3]. Otherwise, these voltage changes can be measured with extracellular electrodes positioned almost in contact with the cell. The quality of the recorded signal depends on the cell-electrode distance and the electrode characteristics. The extracellular recording is an indirect measurement of the ionic movements in a conductive medium like the extracellular compartment. Recorded signals can reflect the fast spike activity of individual neurons or the slower action potentials and synaptic potentials resulting in waves of high amplitude typically from hundreds of microvolt to 1–2 mV of neuronal networks [4]. Indeed, the recording of the action potential generated by the electrical potential of cells could help to identify the cell electrophysiological behavior, to better understand the communication between neuronal networks, e.g., the analysis of neuronal action potential allows

Manuscript received 24 May 2023; revised 16 August 2023; accepted 4 September 2023. Date of publication 15 September 2023; date of current version 16 October 2023. The associate editor coordinating the review of this article and approving it for publication was Dr. Chang-Soo Kim. *(Corresponding author: Ileana Armando.)*

The authors are with the Department of Information Engineering, University of Brescia, 25123 Brescia, Italy (e-mail: i.armando@unibs.it; michela.borghetti@unibs.it; emilio.sardini@unibs.it; mauro.serpelloni@unibs.it).

Digital Object Identifier 10.1109/JSEN.2023.3313652

to understand the functionality of the neuron itself or a group of neuronal cells. Furthermore, to study the response of the action potentials because of both pathological and physiological conditions. This technique allows the recording of neuronal activity both in vitro and in vivo, providing insight into patterns of action potentials in various areas of the nervous system. Multiple neuronal locations can be monitored simultaneously, providing a screening of neuronal population activity and synchronous behaviors within a neuronal network [5]. Micro-electrode arrays (MEAs) are a key component for electrophysiological monitoring in several applications, from in vitro toxicity studies [6] to implantable brain-machine interfaces [7]. Such bioelectronic devices are composed of a grid of tightly spaced electrodes to record the electrogenic cells. MEAs are generally employed to acquire extracellular signals [8], and rarely provide electrophysical stimuli able to provide physiological conditions for maturation [9], [10], [11]. The novel realization of bioelectric systems for the detection and assessment of cells, as well as the standardization and automation of tissue engineering processes, are crucial for the development of automated cell and tissue handling devices [7], [8]. Nowadays, microfabrication techniques are the most common methods for the fabrication of MEAs due to the possibility of electrode dimensions of 10–100 μm with thousands of microelectrodes but they are expensive concerning time and cost production [12], [13], [14], [15], [16]. This leads to the reuse and extending the lifetime of MEA with a decrease in the quality of recorded signals. Furthermore, another major disadvantage of a standard MEA is the fixed position of electrodes and the lack of a customized MEA design for the adaptability to different architectures of a specific neuronal network [17], [18], [19]. Driven by the recent progress in the understanding of neuronal physiology, the development of MEAs with customization properties and low cost and time consumption has gained considerable importance. Therefore, alternative production techniques to overcome these limitations are exploited for the development of MEA [6], [9], [20]. Aerosol jet printing (AJP) is an innovative additive manufacturing (AM) technique that allows the printing of sensors and electronic components with important advantages, such as easy accessibility for prototyping and low-volume manufacturing, processing of varied biocompatible materials, sustainability, and device customization. In particular, the possibility to print electrodes and sensors directly on the medical device allows the development of easily and low-cost prototypes with good resolution, repeatability, and accuracy [21], [22]. It is a feasible technique that allows printing inks with different electrical and chemical properties on a wide range of substrates. AJP performance allows the printing object of micro dimension. Furthermore, AJP provides a selective deposition both on planar and 3-D structures, without using masks or post-processing, and realizing specific surface features [23]. Such technique is also used for biomedical applications [23], [24]. AJP, like other printing technologies, have enabled the evolution of printed and flexible electronics and the use of conductive biocompatible materials, such as poly(3,4-ethylenedioxythiophene)-poly (styrenesulfonate) (PEDOT:PSS), a polymeric material that has excellent properties in terms of conductivity, processability, and stability. Its biocompatibility and conductivity ensure that the PEDOT:PSS can be used safely in biomedical devices as a coating layer for metallic material [25]. Furthermore, due to its higher surface area, the PEDOT:PSS improves the signal-to-noise ratio (SNR) of recorded action potential signal [14]. AJP technique has already been adopted for in vitro tissue engineering applications, e.g., realization of MEA for biocomponent detection of dopamine and other biological components [12] to develop an array of electrodes with dimensions not suitable for action potential recording. In addition, the feasibility related to AJP technique gives the possibility to print biological components, e.g., proteins and ligands. And, in specific MEA applications, this gives the possibility to selectively print ligands in order to create a tailored architecture with a selective coating to promote cell adhesion [26], [27]. Likewise, AJP has also been employed in combination with 3-D printing techniques such as stereolithography to develop MEA for the recording of action potential signals or bioelectronic devices [13], [28]. This work proposes the use of AJP technology as a means of customized and low-cost fabrication of MEAs for both recording action potential signals and stimulating electrically the biological cells, using suitable ink to improve the MEA performance. Furthermore, in this application, the AJP technique gives the possibility to easily realize different geometry according to computer aided design (CAD) and to allow rapid design changes with scalable fabrication according to the need regarding the purpose of the study to develop tailored MEA according to biological cell architecture. In the specific, the focus of this work is the design, fabrication, and geometrical and electrical characterization of a fully AJP-printed MEA. The design of the MEA is fundamental for the realization of a bioelectronic device in agreement with the principal requirements needed for action potential recording. In addition, the customization of the electrodes position is promoted by the employment of AJP compared to traditional MEA fabrication. The fully AJP-printed MEA can achieve the microscopic size of electrodes suitable for such biomedical applications due to the resolution of the AM technique compared to other printing techniques. Furthermore, the opportunity to use conductive polymer opens up the handle of proper material with appropriate mechanical and biological properties for applications with biological materials (e.g., cells, tissue, biological molecules). Finally, the employment of the two conductive inks, the silver ink selected due to the high conductivity properties and the coating of the PEDOT:PSS, in order to promote and enhance the biointerface between the neuronal cells, and the use of AJP, ensure a better signal quality and spatial resolution, and alignment of the different printed layers compared to other AM techniques [14], [29].

II. Sensor Fabrication

A. Design of MEA and Material Selection

The image of the MEA is shown in Fig. 1. The MEA electrode layout was an array of 4 × 4 sensing electrodes of 50 μm diameter with a total distribution of the recording sensitive area of 1–2 mm^2. This sensitive area is considered the

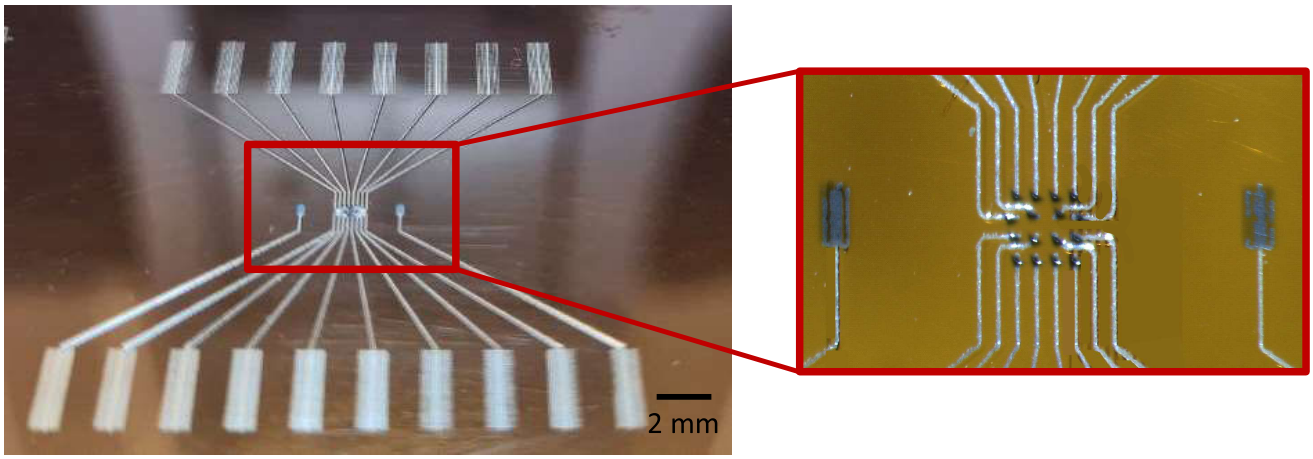

Fig. 1. Photograph and detail of the printed MEA, composed of the contact pad to connect to the electronic front-end.

optimal choice in [4], [5], [6], and [7]. Regarding the number of electrodes, 16 were considered enough to exploit the action potential study generated by electrogenic cells and validate the proposed solution as a proof of concept. The layout was defined according to the ability of AJP technology to realize close and thin geometric elements. The sensing electrode diameter must be comparable to the cell size (4–100 μm in diameter), in order to obtain an improved response of singular neuronal cells, while the distance between the electrodes must be greater than the cell size, according to [8]. Therefore, the dimension of the single electrodes was designed with a diameter of 50 μm according to the requirements for MEA fabrication. While the interelectrode distance was defined as 250 μm according to intrinsic AJP specifications and electrode geometry range. Furthermore, two shared reference electrodes, necessary for both electrical stimulation and action potential recording, were designed on both sides with larger dimensions (400 $\times$ 700 μm) with respect to the electrode array. Then, 18 conductive tracks and their corresponding contact pads (4 $\times$ 1.2 mm) were designed to connect the MEA electrodes with the electronic front-end. The distance between contact pads was designed with pitch of 2.54 mm to connect with specific standard connector. Finally, the overall dimension of the printed MEA complies with the biologists' request to optimize the volume, and consequently, the costs of biological compounds (i.e., cell culture medium and grow factors for promoting cell maturation).

In a previous study [30], due to the novelty of the AJP technique adopted in the MEA fabrication and to provide a customized design able to detect neuronal action potential signals, several computational simulations were performed to investigate the optimal design of the printed electrode array and to satisfy the MEA requirements by using Comsol Multiphysics, a finite element method (FEM) [13]. In particular, the in-silico models provide satisfactory results regarding the dimensions of the sensing electrode and interelectrode distance, proving a proper measurement of the action potential signal. Another crucial part was the definition of a sufficient thickness of the passivation layer for correct isolation and limit signal crosstalk. Several in silico studies (see [30], [31], [32]) were performed to explore the crosstalk in polymer MEA and to predict interference in the signal recording. According to [11], a single insulation layer is enough to reduce significantly the crosstalk and measure correctly the action potential signals produced by neuronal cells. Furthermore, in order to minimize the crosstalk in the printed MEA, two reference electrodes with large overall dimensions were added in the layout proposed in [32]. Finally, the sensing electrodes should be coated with a conductive layer that reduces the electrode impedance for signal crosstalk minimization and low noise.

The proposed design of the MEA is a multilayer structure composed of three different layers. The pattern of each layer was realized by using CAD software to create precise 2-D drawings, AutoCAD. The output file was then converted into a file with customized software for AJP printer movements, that allow the manufacturing process. The possibility to generate personalized 2-D drawings brings customization of the geometry of electrodes and the dimensions in order to realize a customized device for recording action potentials.

Biocompatibility and no corrosion of the selected materials are important for MEA realization. Kapton was preliminarily selected as a substrate for the MEA for adhesion properties and ease of handling. Though the final goal will be the printing directly on the cell culture chamber, after the optimization of the design and the fabrication processes. Since MEA will be printed directly on the culture chamber, the ink selection was oriented more toward the kind of inks that can also be cured by alternative methods avoiding high temperatures so as not to deteriorate the mechanical properties of the culture chamber. Smart Aerosol Conductive Ink (S-CS61308, Genesink, France)—an ink based on silver nanoparticles and suitable for AJP—was selected for the conductive tracks because it is appropriate for MEAs, which require high conductivity for the signal recording and very low curing temperatures. Furthermore, it was selected for the possibility to obtain same value of resistivity both with oven curing and flash lamp annealing (FLA) without damaging the substrate. However, such silver ink has cytotoxic properties and in an aqueous

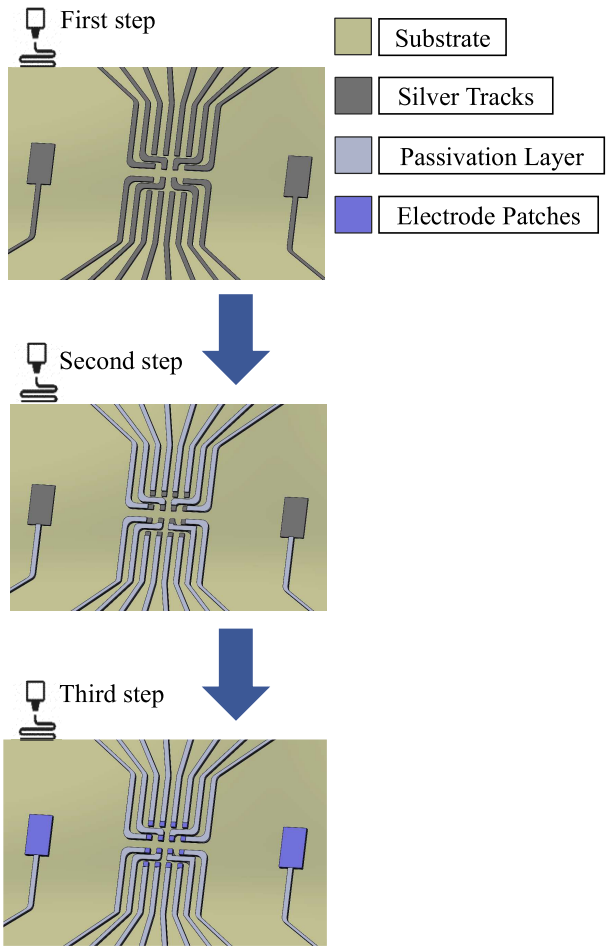

Fig. 2. Rendering of the fabrication process. In the first step, the printing of silver tracks was performed; in the second, the passivation layer was deposited and finally, the electrode patches were printed in the third step.

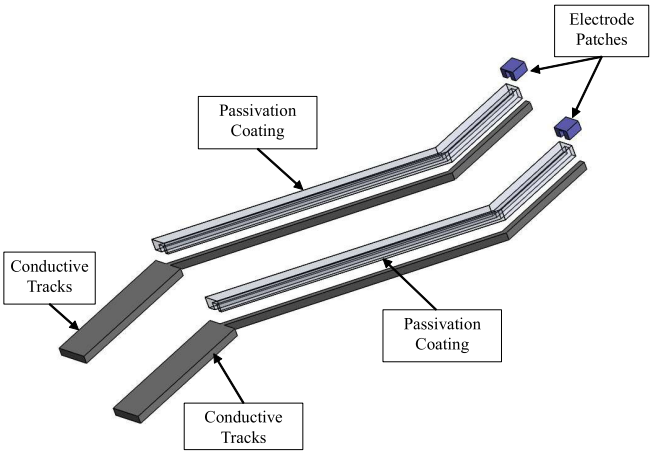

Fig. 3. Detail of the schematic drawing of the MEA. Two tracks of the MEA are represented to show the different layers composed of electrode patches, passivation coating, and conductive tracks.

TABLE I
FABRICATION PARAMETERS IMPOSED FOR AJP TECHNIQUE

Parameter	Pneumatic Mode	Ultrasonic Mode
	Genesink	*NOA 81*
Sheath gas flow (SCCM)	100	40
Atomizer gas flow (SSCM)	635	1395
Exhaust gas flow (SCCM)	620	1365
Atomizer current (mA)	/	/
Plate temperature (◦C)	60	/

Process flows are expressed in the unit standard centimeter cube per minute (SCCM)

environment undergoes corrosion effects, so a layer with insulating and biocompatible material was added. Norland Optical Adhesive 81 (NOA 81)—a UV-curable polymer—was chosen as the passivation layer to shield the silver tracks from the aqueous environment for the survival of the living cells. Besides being a good electrical insulator, it is a transparent and biocompatible material. Orgacon IJ-1005—an ink PEDOT:PSS—was chosen as a biocompatible and conductive surface coating for electrodes (third layer). The printed PEDOT:PSS-based pads act as an interface between biological environment (electrolyte solution/biological cells) and silver tracks to prevent a cytotoxic effect of silver ink on cells. Furthermore, the choice of PEDOT:PSS was also fostered according to lower Young's module compared to metal inks in order to obtain a physiological-like substrate and a low impedance value to improve the SNR. Finally, PEDOT:PSS and NOA 81 inks will be exposed to the electrolyte solution.

B. Fabrication of the MEA

A schematic representation of the proposed fabrication process is shown in Figs. 2 and 3.

The fabrication process consists of three separate depositions: 1) the 18 silver tracks and pads, including the two reference electrodes onto a substrate; 2) the passivation layer on the top of the conductive tracks, leaving uncovered the ends of the conductive tracks in order to obtain the 18 electrodes (16 sensing electrodes and two references) in the center of the device and the contact pads to allow the electrical connections with the electronic front-end for the stimulation and recording of the signals; and 3) a coating and conductive layer over the 16 sensing electrodes and the two reference electrodes. Each step includes deposition and a dedicated curing phase.

In this work, an Aerosol Jet printer, AJ 300 printer (Optomec, Albuquerque, NM, USA) was used to fabricate the MEA. The pneumatic atomizer mode was used for the deposition of silver-based ink and a passivation layer (viscosity of 300 cP at 25 °C.), while the ultrasonic atomizer mode was employed for the deposition of PEDOT:PSS electrodes, due to the viscosity of the conductive polymer (7–12 cP at 22 °C). The printhead nozzle was selected with 200 μm of diameter. The parameters for the fabrication of MEA using AJP are listed in Table I.

For each type of deposition, the printing process was repeated several times to increase the thickness of the printed feature and according to the design requirements. For the coating of the sensing electrodes with PEDOT:PSS, the AJP software script was modified in order to keep the shutter opened for imposed seconds over each silver electrode, building a micropillar over each silver electrode.

The silver tracks were sintered at 150 °C for 1 h in Thermo-Scientific VACUTherm Oven (Thermo Electron LED GmbH, Langenselbold, Germany) to reach the required conductivity,

as recommended by the manufacturer. NOA81 was cured during the printing procedure using UV light by LED Spot type Panasonic, 5% of the maximum peak intensity as selected power. Finally, the PEDOT:PSS-based patches were thermally cured at 130 °C for 6 min in the oven, as recommended by the manufacturer.

III. Results

A. Geometrical Characterization

The in-house tests were carried out to assess the geometrical features and the electrical properties of the printed tracks that composed the multilayer.

The geometrical characterization was performed on four MEAs. In particular, the geometrical size features of printed layers, e.g., thickness and width, were measured by using an optical profilometer, Filmetrics Profilm3D (Filmetrics Inc., 10655 Roselle St., San Diego, CA, USA). The profiles of features acquired with the profilometer were elaborated with specific filters to increase the quality of the profile, and then the geometrical parameters (width and maximum thickness) were measured. Three filters provided by the software Profilm3D were used to reduce the acquisition noise, such as the outliers and the artifacts produced by the profilometers. One filter removes outlying data points from the surface by comparing them against the nearest neighboring points. The second filter based on a three-point leveling method performs a better-quality acquisition of the planar substrate. The third filter fills the invalid pixels using values interpolated/extrapolated from surrounding data.

Fig. 4(a) shows the profile analysis of silver (in red) and NOA 81 (in blue) tracks. For each track, four cross sections equidistant from each other were considered for the profile analysis (the overall number is 128, considering all the printed tracks and tested MEAs). The red line is the mean cross section of the silver tracks, while the shadow red area is the standard deviation. The thickness of silver tracks measures (5.5 $\pm$ 0.6) μm and the width measures (68 $\pm$ 1.4) μm. These tests demonstrate the optimal overlapped silver layer deposition according to geometrical features. The correct overlap is important to ensure uniformity of the thickness of printed track and therefore of the resistivity as well, and to avoid shortcuts between the silver paths of the entire design. Finally, Fig. 4(a) shows a complete coating of silver tracks with NOA 81, whose overall thickness is (33.4 $\pm$ 1.4) μm. This thickness value does not involve a damage to the cells or reorientation due to morphology of substrate according to [33], [34], and [35]. In Fig. 4(b), the profile analysis of sensing electrodes is shown. The thickness of PEDOT:PSS micropillars is (0.8 $\pm$ 0.2) μm. The PEDOT:PSS coating over silver ink results to be a micrometer layer and cover all the silver area. The several measurements and acquisitions with profilometer demonstrated that the silver ink was completely coated by PEDOT:PSS, both on sensing electrodes and reference electrodes.

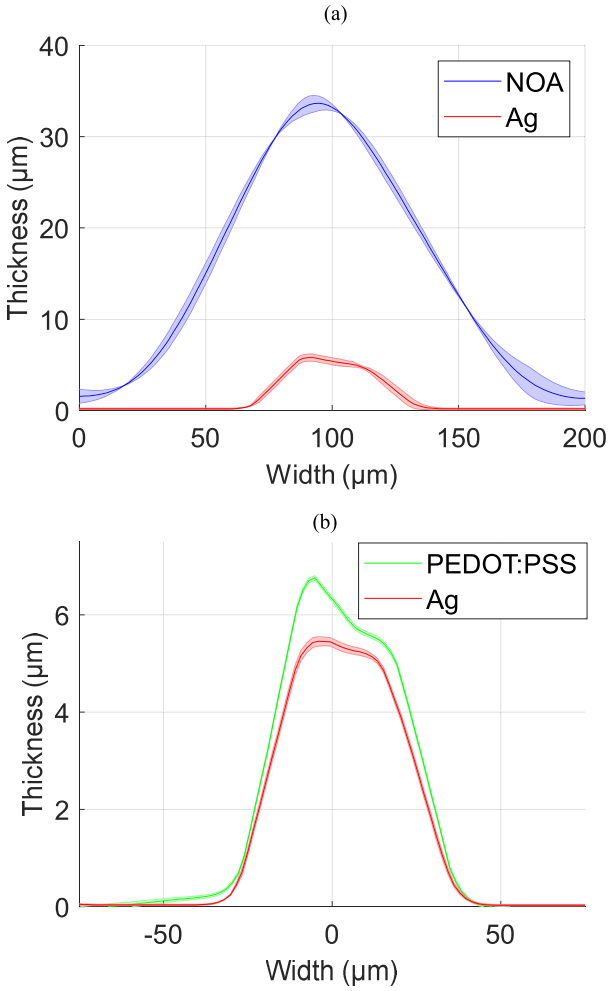

Fig. 4. (a) Average profile of silver tracks (solid red line) and coating made by NOA 81 tracks (blue solid line). The shadow area is the standard deviation calculated on 128 profiles acquired from the four MEAs. (b) Average profile of PEDOT:PSS coating (solid green line) and underlying silver layer (solid red line). The shadow area is the standard deviation calculated on 64 profiles of the sensing electrodes acquired from the four MEAs.

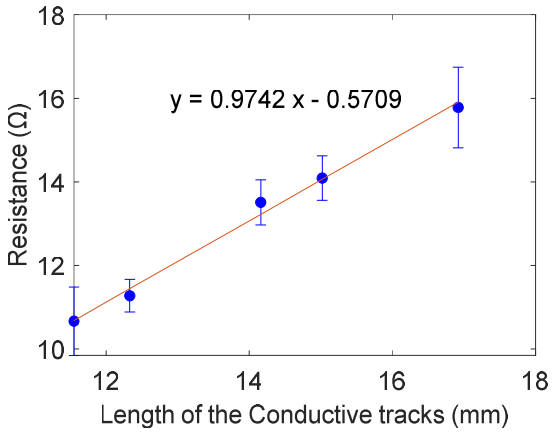

Fig. 5. Plot of the measured resistance value for different conductive tracks length with mean values and standard deviation calculated on at least eight tracks, considering all four MEAs.

B. Electrical Characterization

The evaluation of the electrical properties of the silver tracks was performed employing a test bench multimeter (HP34401A, Agilent). The mean value (dots) and the standard deviation (error bars) of the resistance were reported in the y-axis of Fig. 5, according to the different lengths of the tracks

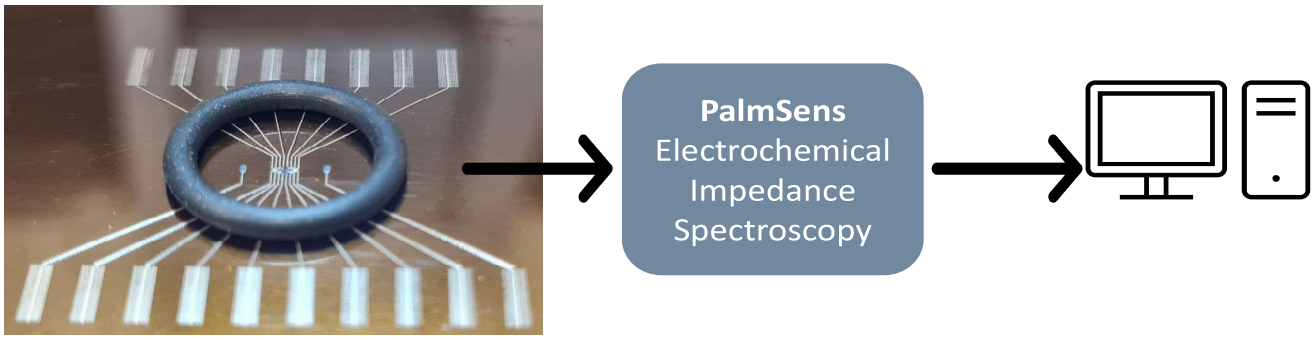

Fig. 6. Experimental setup used for the EIS. The sensor is filled with PBS and then, the PalmSens is connected to the sensor and the measurement are performed and data send to a computer for the data analysis.

in the x-axis. In each MEA, 17.4 mm is the length of the two tracks for the reference electrodes, while the other values are the four tracks with the same length, due to the symmetrical layout. The resistance, as expected, increases proportionally with the length of the conductive tracks.

The resistivity ρ was calculated considering the several resistance R measurements by using the following equation:

$$\rho = R \cdot (w \cdot t)/l \tag{1}$$

where w is the average width of the tracks, t is the average thickness, and l is the length of the measured conductive track resistivity.

The mean value for the silver ink calculated from (1) was 5.7 $\mu\Omega * \text{cm}^2$ and it agrees with the manufacturer datasheet of 5.75 $\mu\Omega * \text{cm}$ [36].

The long-term stability and the reusability of the MEAs, in particular the PEDOT:PSS electrodes were evaluated by means of electrochemical impedance spectroscopy (EIS) for up to two weeks. The setup is shown in Fig. 6. An o-ring was glued on the Kapton substrate to surround the printed MEA and build the chamber wall for containing phosphate-buffered saline (PBS), which simulates cell culture medium [14]. EIS was performed with a commercial portable potentiostat (PalmSens 3 PS Trace, PalmSens BV, Netherlands), controlled using dedicated software (PS Trace 5.3). The EIS measurements were performed in the frequency range of 0.01 Hz–10 kHz, with ac-amplitude of 50 mVrms and dc bias of to 0 V. In accordance with the typical range relevant for detecting local field potentials (1–300 Hz) and extracellular action potentials (300 Hz–10 kHz) [3], the acquisition window was reduced. The impedance was always measured between each MEA sensing electrode and the closer reference electrode. Each measurement consisted of ten repetitive scans, one time a day for two weeks. For the equivalent model fitting was used the tool included in commercial potentiostat, PS Trace. The phase of the impedance is not reported, since for the evaluation of reusability and stability in long-term analysis this is not relevant, as reported in previously works [14], [29], [37]. Regarding the reusability test, the chamber MEA was covered with 40 μL of PBS and ten measurements were repeated before removing the PBS. Several washes were performed to clean the sensor with distilled water, to remove the ionic solution. This procedure was repeated every day for two

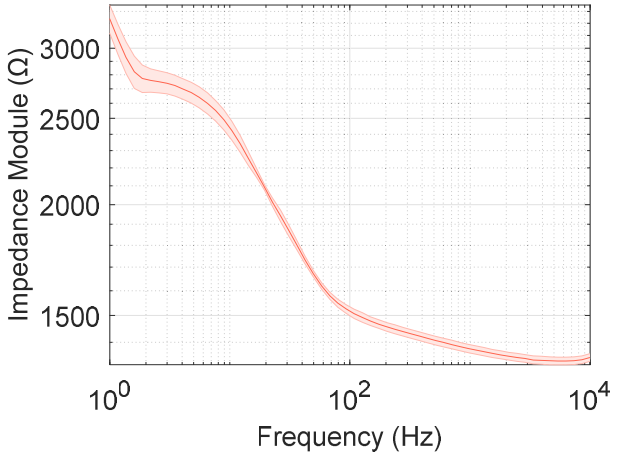

Fig. 7. Impedance magnitude change over frequency (reusability test) on 14 days. Error bars show the standard deviation on two MEAs. The impedance was measured between the electrodes and the reference electrodes.

weeks on two MEAs. The plot in Fig. 7 shows the mean impedance magnitude (solid line) and its standard deviation (shadow area) calculated on all performed measurements on 14 days over the frequency sweep. The impedance at 1 kHz has a value of (1370 $\pm$ 30) Ω, which is significantly below the value of 160 kΩ measured on the simplest commercially available MEAs with gold electrodes [38]. At 100 Hz, the impedance slightly increases to (1500 $\pm$ 104) Ω but still lower than commercially available MEAs. The impedance evaluation confirms that PEDOT:PSS improves the electrode solution interface. The lower impedance values with respect to commercial MEAs ensure the printed MEA electrical compatibility with the commercial front-end for stimulation and recording.

For stability evaluation, 60 μL of PBS was used to fill the chamber without removing the solution, until the end of the test. All the measurements were performed at room temperature and in humidity-controlled conditions to limit the evaporation of the liquid solution and keep stable testing conditions, in accordance with [37]. The measurements were performed at two fixed frequencies 100 Hz and 1 kHz, in order to provide a comparison to [11]. Fig. 8 shows the change of impedance magnitude during the 14 days at frequencies of 100 Hz and 1 kHz. The impedance at 1 kHz was observed due to the extensive use in characterization of neuronal electrodes [11]. The impedance range is in line with the

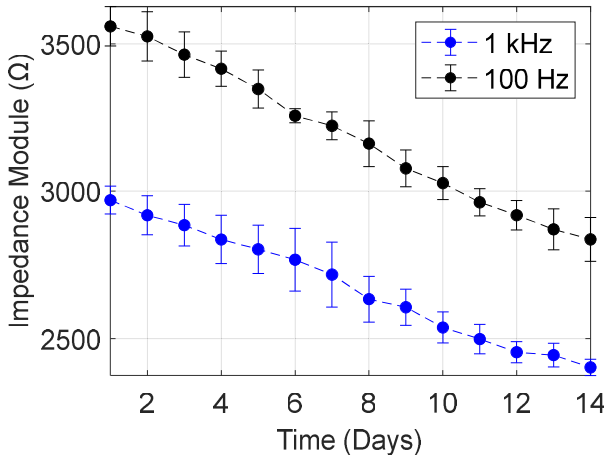

Fig. 8. Impedance magnitude over 14 days in PBS for the stability of two sensor at frequency of 100 Hz and 1 kHz. Error bars show the standard deviation of two MEAs.

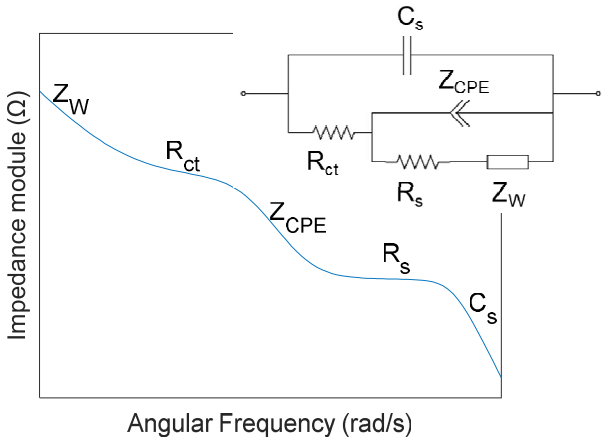

Fig. 9. Theoretical impedance module according to frequency variations for the randles circuit model (in the inset) for the electrode/electrolyte interface used for the fitting of the experimental results.

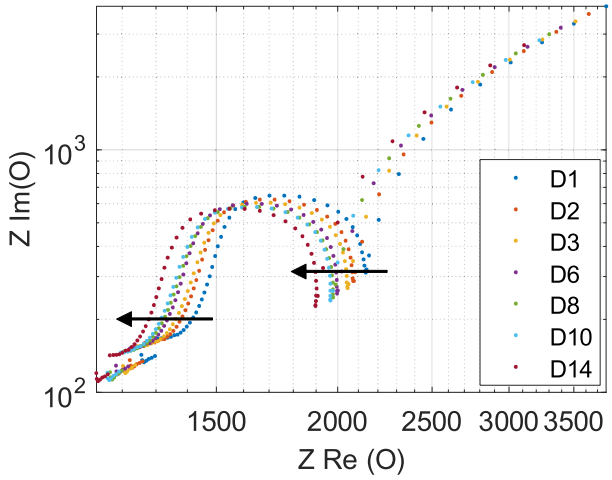

Fig. 10. Nyquist plot with real and imaginary part of the experimental results obtained in the stability test of the printed MEA within two weeks.

literature. After two weeks in PBS, the impedance magnitude is (2680 ± 654) Ω at 1 kHz, which is well below the value observed in the reported article [14] after two weeks in the medium. Furthermore, the impedance magnitude decreases over time in both 100 Hz and 1 kHz, due to evaporation of solution. In the next paragraph, we discuss the issue. The devices exhibited a small decrease in impedance values, which ensures low degradation of PEDOT:PSS coating as confirmed in [37]. This ensures optimal recording signals for future applications.

The impedance measurement can be modeled as an equivalent circuit in which each component can be related to a particular electrochemical process. The impedance magnitude presented a behavior in agreement with the theory (shown in Fig. 9) concerning the EIS of ionic liquid measurement [39]. At high frequencies, the solution characteristics dominate on impedance plot with an RC effect that depends on concentration of ions in PBS solution. While the double-layer capacitance was modeled as a capacitor C_{dl} in series to R_s, the surface nonidealities were modeled by constant phase element (CPE). A charge transfer resistance R_{ct} is defined according to charge transfer process that allows transferring electrons from electrode to solution (or vice-versa). Finally, at low frequencies, the predominant component regarding the diffusion of the ions was modeled by the Warburg impedance Z_W, which corresponds to a line at a phase angle of 45° in the complex plane plots [40]. Comparing the theory module of impedance shown in Fig. 9 with the results presented in this work in Fig. 7, at low frequency, before the frequency of 1–2 Hz, we have a phase angle higher than 45°, apparently inconsistent with the theory. Such difference was due to the thickness of PEDOT:PSS layer, as described in [41], which was shown for different depositions times (and thus thickness), a variation of the slope at low frequency, with a variation of the value of Warburg element. Finally, the equivalent model evaluation was useful for monitoring the behavior of the electrochemical system for long-term analysis. The change in the value of the electronic elements indicated modifications of the electrochemical properties of the cell, particularly interesting for the long-term stability analysis.

The Nyquist plots of EIS measurements obtained from the stability test (see Fig. 10) show a decrease in solution resistance over time due to the decrease of solution resistance induced by evaporation of the water. Such variation explains the behavior of the curve within the 14 days in Fig. 8, where the value of the impedance decreases according to the days as a result of the water evaporation that has a predominant effect. Furthermore, in [42], it is possible to see a decrease in the impedance magnitude in long-term analysis, before an initial impedance increase. According to this work, some modifications of electrode surface could bring to a decrease of impedance magnitude.

The shape of the curve remained the same with no variation in the electrochemical elements of the equivalent model.

IV. Conclusion

The article proposed AJP as an enabling technology for the fabrication of printed MEAs used for electrical stimulation and real-time monitoring of the action potential signals. The realization of a low-cost and multilayer device by using suitable and biocompatible inks to improve the sensor

performance is described. Furthermore, the work proposes itself as an alternative to the traditional microfabrication techniques that allow the customization of the electrode design according to neuronal network architecture. The achieved printed MEAs, in this current design and fabrication process, are the result of an improvement of a previous work [43]. After the design and the fabrication by using AM technique, the printed devices were then characterized both in terms of geometrical and electrical properties. Stability and reusability were both tested to evaluate the performance of sensor for long-term analysis. The results are promising upon the literature, in terms of customization of electrode design and feasibility of a low-cost 3-D printing technique with advanced flexibility and reproducibility. Furthermore, the possibility to improve the electrical stimulation with suitable electrode design and position, to enhance and to accelerate cell maturation protocol, and, at the same time, to provide a real-time monitoring device for maturation of neuronal activity during cell culture. This printed MEA, as proof of concept, is an important starting point for realization of a customized and sensorized system to improve in vitro cell culture. The advanced deposition and curing methods of electrodes, passivation layer, and conductive tracks allow direct integration into cell culture device in future applications. Furthermore, the customization offered by AJP technique suggests different opportunities, such as the possibility of selectively depositing cell adhesion protein to create a specific architecture for neuronal network. Furthermore, the integration of other sensors (e.g., lactate, pH) could provide complementary information about cell culture activity, providing a completely monitoring system. And finally, in the future, the biocompatibility and the functionality of the printed MEA will be tested by adding electronic front-end for stimulation and recording of action potential and seeding neuronal cells onto the device.

REFERENCES

[1] J. M. Keller and M. Frega, "Past, present, and future of neuronal models in vitro," *Adv. Neurobiol.*, vol. 22, pp. 3–17, May 2019.

[2] A. Pelkonen et al., "Functional characterization of human pluripotent stem cell-derived models of the brain with microelectrode arrays," *Cells*, vol. 11, no. 1, p. 106, 2022.

[3] N. Graziane and Y. Dong, "Extracellular and intracellular recordings," in *Electrophysiological Analysis of Synaptic Transmission* (Neuromethods), vol. 187. Humana Press, 2022, pp. 3–15, doi: 10.1007/978-1-0716-2589-7_1.

[4] M. E. Spira and A. Hai, "Multi-electrode array technologies for neuroscience and cardiology," *Nature Nanotechnol.*, vol. 8, no. 2, pp. 83–94, Feb. 2013.

[5] V. L. Da Silveira Nantes Button, "Chapter 2—Electrodes for biopotential recording and tissue stimulation," in *Principles of Measurement and Transduction of Biomedical Variables*. Academic, 2015, pp. 25–76, doi: 10.1016/B978-0-12-800774-7.00002-7.

[6] G. Melle et al., "Intracellular recording of human cardiac action potentials on market-available multielectrode array platforms," *Frontiers Bioeng. Biotechnol.*, vol. 8, pp. 1–10, Feb. 2020.

[7] G. Kim et al., "Recent progress on microelectrodes in neural interfaces," *Materials*, vol. 11, no. 10, p. 1995, Oct. 2018.

[8] L. Xu et al., "Trends and recent development of the microelectrode arrays (MEAs)," *Biosensors Bioelectron.*, vol. 175, Mar. 2021, Art. no. 112854.

[9] H. Yamamoto, L. Grob, T. Sumi, K. Oiwa, A. Hirano-Iwata, and B. Wolfrum, "Ultrasoft silicone gel as a biomimetic passivation layer in inkjet-printed 3D MEA devices," *Adv. Biosystems*, vol. 3, Sep. 2019, Art. no. 1900130.

[10] S. Ronchi et al., "Single-cell electrical stimulation using CMOS-based high-density microelectrode arrays," *Frontiers Neurosci.*, vol. 13, pp. 1–17, Mar. 2019.

[11] S. F. Cogan, "Neural stimulation and recording electrodes," *Annu. Rev. Biomed. Eng.*, vol. 10, pp. 275–309, Aug. 2008.

[12] H. Yang, M. T. Rahman, D. Du, R. Panat, and L. Yuehe, "3-D printed adjustable microelectrode arrays for electrochemical sensing and biosensing," *Physiol. Behav.*, vol. 230, no. 12, pp. 600–606, 2017.

[13] A. Kundu, C. Nattoo, S. Fremgen, S. Springer, T. Ausaf, and S. Rajaraman, "Optimization of makerspace microfabrication techniques and materials for the realization of planar, 3D printed microelectrode arrays in under four days," *RSC Adv.*, vol. 9, no. 16, pp. 8949–8963, 2019.

[14] L. D. Garma, L. M. Ferrari, P. Scognamiglio, F. Greco, and F. Santoro, "Inkjet-printed PEDOT: PSS multi-electrode arrays for low-cost: In vitro electrophysiology," *Lab Chip*, vol. 19, no. 22, pp. 3776–3786, 2019.

[15] J. Rivnay, H. Wang, L. Fenno, K. Deisseroth, and G. G. Malliaras, "Next-generation probes, particles, and proteins for neural interfacing," *Sci. Adv.*, vol. 3, no. 6, Jun. 2017, Art. no. 1601649.

[16] J. Schnitker et al., "Rapid prototyping of ultralow-cost, inkjet-printed carbon microelectrodes for flexible bioelectronic devices," *Adv. Biosyst.*, vol. 2, no. 3, pp. 1–9, 2018.

[17] M. Schürmann et al., "Technical feasibility study for production of tailored multielectrode arrays and patterning of arranged neuronal networks," *PLoS ONE*, vol. 13, no. 2, pp. 1–20, 2018.

[18] J. Ji, X. Ren, and P. Zorlutuna, "Cardiac cell patterning on customized microelectrode arrays for electrophysiological recordings," *Micromachines*, vol. 12, no. 11, p. 1351, Oct. 2021.

[19] N. Gaio et al., "Cytostretch, an organ-on-chip platform," *Micromachines*, vol. 7, no. 7, pp. 1–14, 2016.

[20] M. Ribeiro, P. Ali, B. Metcalfe, D. Moschou, and P. R. F. Rocha, "Microfluidics integration into low-noise multi-electrode arrays," *Micromachines*, vol. 12, no. 6, pp. 1–9, 2021.

[21] T. Han, S. Kundu, A. Nag, and Y. Xu, "3D printed sensors for biomedical applications: A review," *Sensors*, vol. 19, no. 7, p. 1706, Apr. 2019.

[22] D. Maddipatla, B. B. Narakathu, and M. Atashbar, "Recent progress in manufacturing techniques of printed and flexible sensors: A review," *Biosensors*, vol. 10, no. 12, p. 199, Dec. 2020.

[23] N. G. D. Novo, E. Cantù, S. Tonello, E. Sardini, and M. Serpelloni, "Support-material-free microfluidics on an electrochemical sensors platform by aerosol jet printing," *Sensors*, vol. 19, no. 8, p. 1842, Apr. 2019.

[24] S. Tonello et al., "Impedance-based monitoring of mesenchymal stromal cell three-dimensional proliferation using aerosol jet printed sensors: A tissue engineering application," *Materials*, vol. 13, no. 10, p. 2231, May 2020, doi: 10.3390/ma13102231.

[25] A. K. Waafi, N. Gaio, W. F. Quiros-Solano, P. Dijkstra, P. M. Sarro, and R. Dekker, "Low-impedance PEDOT: PSS MEA integrated in a stretchable organ-on-chip device," *IEEE Sensors J.*, vol. 20, no. 3, pp. 1150–1157, Feb. 2020.

[26] A. J. Capel et al., "Digitally driven aerosol jet printing to enable customisable neuronal guidance," *Frontiers Cell Develop. Biol.*, vol. 9, pp. 1–16, Aug. 2021.

[27] N. E. Sanjana and S. B. Fuller, "A fast flexible ink-jet printing method for patterning dissociated neurons in culture," *J. Neurosci. Methods*, vol. 136, no. 2, pp. 151–163, Jul. 2004.

[28] M. S. Saleh et al., "CMU array: A 3D nanoprinted, fully customizable high-density microelectrode array platform," *Sci. Adv.*, vol. 8, 2022, Art. no. eabj4853, doi: 10.1126/sciadv.abj4853.

[29] B. Bachmann et al., "All-inkjet-printed gold microelectrode arrays for extracellular recording of action potentials," *Flexible Printed Electron.*, vol. 2, no. 3, Sep. 2017, Art. no. 035003.

[30] I. Armando, M. Borghetti, E. Sardini, and M. Serpelloni, "A computational model for the design optimization of multi-electrode arrays by aerosol-jet printing," *Proc. CIRP*, vol. 110, pp. 87–92, 2022.

[31] Y. Qiang et al., "Crosstalk in polymer microelectrode arrays," *Nano Res.*, vol. 14, no. 9, pp. 3240–3247, Sep. 2021.

[32] J. R. Naughton et al., "Suppression of crosstalk in multielectrode arrays with local shielding," *Frontiers Nanotechnol.*, vol. 4, pp. 1–11, Aug. 2022.

[33] K. Yang et al., "Electroconductive nanoscale topography for enhanced neuronal differentiation and electrophysiological maturation of human neural stem cells," *Nanoscale*, vol. 9, no. 47, pp. 18737–18752, 2017.

[34] C. Simitzi, A. Ranella, and E. Stratakis, "Controlling the morphology and outgrowth of nerve and neuroglial cells: The effect of surface topography," *Acta Biomaterialia*, vol. 51, pp. 21–52, Mar. 2017.

[35] M. Bramini, A. Rocchi, F. Benfenati, and F. Cesca, "Neuronal cultures and nanomaterials," *Adv. Neurobiol.*, vol. 22, pp. 51–79, May 2019.
[36] *Product Datasheet Smartink Genesink Smart Aeroso*, Genesink, Rousset, France, 2019, p. 2.
[37] T. Ryynänen and P. Kallio, "Microelectrode array designing for dummies: Contribution of the tracks to the impedance behavior and the noise level," in *Proc. IEEE SENSORS*, Oct. 2020, pp. 1–4.
[38] D. A. Koutsouras et al., "Impedance spectroscopy of spin-cast and electrochemically deposited PEDOT: PSS films on microfabricated electrodes with various areas," *ChemElectroChem*, vol. 4, no. 9, pp. 2321–2327, Sep. 2017.
[39] "Allen J. Bard and Larry R. Faulkner, Electrochemical methods: Fundamentals and applications, New York: Wiley, 2001, 2nd ed." *Russian J. Electrochem.*, vol. 38, pp. 1364–1365, 2002, doi: 10.1023/A:1021637209564.
[40] C. M. A. Brett, "Electrochemical impedance spectroscopy in the characterisation and application of modified electrodes for electrochemical sensors and biosensors," *Molecules*, vol. 27, no. 5, p. 1497, 2022.
[41] A. R. Harris, P. J. Molino, R. M. I. Kapsa, G. M. Clark, A. G. Paolini, and G. G. Wallace, "Correlation of the impedance and effective electrode area of doped PEDOT modified electrodes for brain–machine interfaces," *Analyst*, vol. 140, no. 9, pp. 3164–3174, 2015.
[42] G. Dijk, A. L. Rutz, and G. G. Malliaras, "Stability of PEDOT: PSS-coated gold electrodes in cell culture conditions," *Adv. Mater. Technol.*, vol. 5, Mar. 2020, Art. no. 1900662.
[43] I. Armando, M. Borghetti, E. Sardini, and M. Serpelloni, "Preliminary study on printed microelectrode array by aerosol jet printing technology," in *Proc. IEEE Int. Workshop Metrology Ind. 4.0 IoT (MetroInd4.0IoT)*, Jun. 2022, pp. 261–266.

Ileana Armando (Student Member, IEEE) received the M.Sc. degree in biomedical engineering from the Politecnico di Torino, Turin, Italy, in 2019. She is currently pursuing the Ph.D. degree in technology for health with the University of Brescia, Brescia, Italy.

She is working on the printed sensor for biotechnology applications. Her research interests include biosensors and regenerative medicine.

Michela Borghetti (Member, IEEE) received the master's (cum laude) degree in electronic engineering from the University of Brescia, Brescia, Italy, in 2012, the Ph.D. degree from the Universitat Politècnica de Catalunya, Barcelona, Spain, in 2015, and the Ph.D. degree in technology for health from the University of Brescia, in 2016.

She is currently a Postdoctoral Researcher with the Department of Information Engineering, University of Brescia. She is working on the design and fabrication of sensors for healthcare using low-cost technologies.

Emilio Sardini (Senior Member, IEEE) received the M.Sc. degree in electronics engineering from Politecnico di Milano, Milan, Italy, in 1983.

He has been a member of the Academic Senate, Board of Directors, the Deputy Dean of the Engineering Faculty, the Director of the Department of Information Engineering, and a Coordinator of the "Technology for Health" Ph.D. Program, University of Brescia, Brescia, Italy, where he is currently a Full Professor with the Department of Information Engineering. His research interests include electronic instrumentation, sensors and signal conditioning electronics, and the development of autonomous sensors for biomedical applications.

Mauro Serpelloni (Member, IEEE) received the M.S. (cum laude) degree in industrial management engineering and the Ph.D. degree in electronic instrumentation from the University of Brescia, Brescia, Italy, in 2003 and 2007, respectively.

He is currently a Full Professor with the Department of Information Engineering, University of Brescia. He is Manager of a new laboratory for aerosol jet printing (AJP). His current research interests include biomechatronic systems, contactless transmission, printed electronics, AJP, photonic curing, and signal processing for microelectromechanical systems.

Open Access funding provided by 'Università degli Studi di Brescia' within the CRUI CARE Agreement